Inorganic Chemistry
Article

Inorg. Chem. **2011**, *50*, 345–357 **345**
DOI: 10.1021/ic102028d

Covalent Lanthanide Chemistry Near the Limit of Weak Bonding: Observation of $(CpSiMe_3)_3Ce-ECp^*$ and a Comprehensive Density Functional Theory Analysis of $Cp_3Ln-ECp$ (E = Al, Ga)

Jamin L. Krinsky,*,† Stefan G. Minasian,‡ and John Arnold*,‡

†*Molecular Graphics and Computation Facility and* ‡*Department of Chemistry, University of California, Berkeley, California 94720, United States*

Received October 5, 2010

Experimental evidence for the existence of two new lanthanide-metalloligand adducts $(CpSiMe_3)_3Ce-ECp^*$ (E = Al, Ga) is presented. Paramagnetic ^1H NMR titration experiments were employed to derive thermodynamic parameters for Ce−Ga dative bond formation, and competition experiments with the U analogue were performed. Density functional theory calculations were undertaken using model complexes $Cp_3Ln-ECp$ where Ln = La−Lu and E = Al, Ga. The Ln−E bond distances were predicted to decrease more sharply across the Ln series than those involving hard Lewis bases; however, local increases were observed at Eu and Yb. Electronic analyses were performed in the natural bond orbital-natural localized molecular orbital (NBO/NLMO) formalism, indicating that the E→Ln acceptor orbital is primarily of d character in all cases. The Cp^- ligands donate significant electron density to the Ln d manifold and thus in its bonding interactions with a dative ligand the Ln center may be considered to be Ln^{2+} in the $f^{(n-3)}d^1$ electronic configuration (n = 3 for La, etc.). Molecular dipole moments, NLMO and natural population analyses, bond order indices, measures of E→Ln charge transfer, and calculated Ln−E heterolytic bond disruption enthalpies were found to follow saw-tooth trends, which correlate to varying degrees with the ionization potentials of the Ln^+ ions (corrected for their ground state-to-$f^{(n-3)}d^2$ excitations). It is proposed that a steric-strain component which increases with the lanthanide contraction in this case balances the Ln−E bond stabilizing effect of core-orbital contraction. All data indicate that the Ln−E bonding interactions are predominantly of covalent or nonpolar donor−acceptor character. However, the formation of a strong covalent bond is not observed because of resistance to reduction of an effectively divalent Ln center.

Introduction

The argument regarding the presence of covalent interactions in bonding with the lanthanide metals has not been fully resolved.[1] This debate is worthwhile insofar as a thorough understanding of these elements' properties will facilitate new discoveries in fields ranging from nuclear waste remediation[2] to medical imaging,[3] optical materials,[4] and catalysis.[5] It has been convincingly established that the 4f electrons do not normally contribute to bonding interactions in the lanthanides,[6] for instance the optical f→f transitions of luminescent Ln^{3+} coordination compounds are nearly unperturbed upon modification of the ligand sphere.[7] However, the 5d levels can be available to participate in bonding. This leads to surprisingly strong covalent bonding interactions

*To whom correspondence should be addressed. E-mail: krinsky.jamin@gmail.com (J.L.K.), arnold@berkeley.edu (J.A.).

(1) (a) Raymond, K. N.; Eigenbrot, C. W. *Acc. Chem. Res.* **1980**, *13*, 276–283. (b) Roger, M.; Barros, N.; Arliguie, T.; Thuery, P.; Maron, L.; Ephritikhine, M. *J. Am. Chem. Soc.* **2006**, *128*, 8790–8802. (c) David, F. H. *Radiochim. Acta* **2008**, *96*, 135–144. (d) Roos, B. O.; Pyykkö, P. *Chem.—Eur. J.* **2010**, *16*, 270–275. (e) Arnold, P. L.; Liddle, S. T.; McMaster, J.; Jones, C.; Mills, D. P. *J. Am. Chem. Soc.* **2007**, *129*, 5360–5361. (f) Liddle, S. T.; Mills, D. P.; Gardner, B. M.; McMaster, J.; Jones, C.; Woodul, W. D. *Inorg. Chem.* **2009**, *48*, 3520–3522. (g) Krogh-Jespersen, K.; Romanelli, M. D.; Melman, J. H.; Emge, T. J.; Brennan, J. G. *Inorg. Chem.* **2010**, *49*, 552–560. (h) Kuta, J.; Clark, A. E. *Inorg. Chem.* **2010**, *49*, 7808–7817.

(2) (a) Mazzanti, M.; Wietzke, R. L.; Pecaut, J.; Latour, J. M.; Maldivi, P.; Remy, M. *Inorg. Chem.* **2002**, *41*, 2389–2399. (b) Mehdoui, T.; Berthet, J. C.; Thuery, P.; Ephritikhine, M. *Dalton Trans.* **2004**, 579–590. (c) Mehdoui, T.; Berthet, J. C.; Thuery, P.; Ephritikhine, M. *Chem. Commun.* **2005**, 2860–2862.

(3) (a) Werner, E. J.; Datta, A.; Jocher, C. J.; Raymond, K. N. *Angew. Chem., Int. Ed.* **2008**, *47*, 8568–8580. (b) Caravan, P.; Ellison, J. J.; McMurry, T. J.; Lauffer, R. B. *Chem. Rev.* **1999**, *99*, 2293–2352.

(4) (a) Armelao, L.; Quici, S.; Barigelletti, F.; Accorsi, G.; Bottaro, G.; Cavazzini, M.; Tondello, E. *Coord. Chem. Rev.* **2010**, *254*, 487–505. (b) Moore, E. G.; Xu, J.; Dodani, S. C.; Jocher, C. J.; D'Aléo, A.; Seitz, M.; Raymond, K. N. *Inorg. Chem.* **2010**, *49*, 4156–4166.

(5) (a) Molander, G. A.; Romero, J. A. C. *Chem. Rev.* **2002**, *102*, 2161–2185. (b) Kobayashi, S.; Sugiura, M.; Kitagawa, H.; Lam, W. W. L. *Chem. Rev.* **2002**, *102*, 2227–2302. (c) Seo, S. Y.; Yu, X. H.; Marks, T. J. *J. Am. Chem. Soc.* **2009**, *131*, 263–276.

(6) (a) Maron, L.; Eisenstein, O. *J. Phys. Chem. A* **2000**, *104*, 7140–7143. (b) Freedman, D.; Melman, J. H.; Emge, T. J.; Brennan, J. G. *Inorg. Chem.* **1998**, *37*, 4162–4163; but see: (c) Clavaguéra, C.; Dognon, J. P.; Pyykkö, P. *Chem. Phys. Lett.* **2006**, *429*, 8–12.

(7) Eliseeva, S. V.; Bunzli, J. C. G. *Chem. Soc. Rev.* **2010**, *39*, 189–227.

Published on Web 12/08/2010

between low-valent lanthanides and arenes, wherein valence Ln-centered electrons present in (or promoted to) the d-orbital manifold are partially donated to the arene π-antibonding levels.[8] The importance of the opposite process (dative covalent bonding from a neutral donor ligand to the d levels of a formally high-valent Ln^{3+} center) is still in question and is a difficult problem because in this case a dominant ionic component to bonding will usually mask any covalent contribution. Note that for the purposes of this study we explicitly include dative, charge-transfer interactions in the definition of covalent phenomena.[9] Recent computational evidence strongly suggests that covalent interactions do *not* play a part in Ln^{3+}-water bonding[1h] although an analogously thorough inspection of soft (or polarizable) donor ligands[1b] has not, to our knowledge, been attempted.

As mentioned above, covalency arguments have played a role in the development of efficient actinide/lanthanide separation technologies based on soft-donor atom containing ligands. By exploiting a difference in the availability of An and Ln valence orbitals for bonding,[10] sulfur-based soft donor ligands including bisalkyldithiophosphinic acids such as Cyanex 301 are known to provide separation factors ($S_{An/Ln}$) as high as 5900.[11] The group 13 σ-donor metalloligands Cp*E (Cp* = C_5Me_5; E = Al, Ga),[12] while not applicable to industrial processes, are interesting in that their monovalent metals possess a diffuse lone pair of electrons available for donation to a Lewis acid and yet are much more electropositive than the common neutral donor ligands such as N-heterocyclic carbenes.[13] This feature renders them ideal for studying covalent effects in dative bonding with relatively electropositive metals because of the attenuated ionic bonding component. The electronic structures and properties of CpE are fascinating in their own right and have been investigated by experiment[14] and computation.[15] It has been known for some time that Cp*E ligands form strong dative bonds with soft d-block species such as iron(0).[16] More recently, Roesky prepared a number of adducts with the divalent lanthanocenes which displayed extremely low Ln−E binding energies, although the Cp*Ga (Cp* = pentamethylcyclopentadienyl) complexes were stable toward dissociation in solution.[17]

In a recent report, we extended the coordination chemistry of the trivalent f-block $(CpR)_3M$ species to include the $(CpSiMe_3)_3M-ECp^*$ (M = U, Nd; E = Al, Ga) adducts.[18] These two f-block metals were chosen to allow the use of experimental and theoretical methods to directly compare differences in dative metal−metal bonding between an actinide and its lanthanide congener. The $(CpSiMe_3)_3Nd-ECp^*$ complexes were observed in solution by variable-temperature paramagnetic NMR spectroscopy, and reliable M−E bond disruption enthalpies (*BDE*s) were obtained for $(CpSiMe_3)_3M-GaCp^*$ by that method, although neither Cp*Al nor Cp*Ga adducts with neodymium were isolated. DFT calculations[10a,13b,19] on the model system Cp_3M-ECp with the B3PW91 functional and a small-core effective core potential (ECP) resulted in good agreement with experimental M−Ga *BDE*s of the fully substituted complexes after the addition of an empirically determined correction. Results for the CpAl analogues predicted that the aluminum adducts are more strongly bound than those of gallium (experimentally verified for the uranium adducts and in contrast to the divalent lanthanide work mentioned above) although the Nd−Al *BDE* is lower than the energy required (per Al) to disrupt the competitively formed $(Cp^*Al)_4$ tetramer. Therefore $(CpSiMe_3)_3Nd-AlCp^*$ was predicted to be non-isolable.

We begin the following discussion by presenting the new Ln analogues $(CpSiMe_3)_3Ce-ECp^*$ (E = Al, Ga), which provide additional data points from which to verify trends derived from computational predictions made for other lanthanide analogues. In-depth computational analyses are then presented for the 30 $Cp_3Ln-ECp$ adducts where Ln = La−Lu and E = Al, Ga. Few experimental data are available for exactly isostructural series across the lanthanides,[20] and those that exist have been used mostly in investigating the lanthanide contraction. To our knowledge this is the first study examining a weakly ionic bonding interaction with all trivalent ions in the lanthanide series. The objective of this endeavor is to aid in establishing the extent of, and meaningful trends in, the covalent component of such interactions.

Experimental Details

General Considerations. All reactions were performed using standard Schlenk-line techniques or in an MBraun drybox (< 1 ppm O_2/H_2O) unless noted otherwise. All glassware was

(8) (a) Bochkarev, M. N. *Chem. Rev.* **2002**, *102*, 2089–2117. (b) King, W. A.; Di Bella, S.; Lanza, G.; Khan, K.; Duncalf, D. J.; Cloke, F. G. N.; Fragala, I. L.; Marks, T. J. *J. Am. Chem. Soc.* **1996**, *118*, 627–635. (c) Hong, G. Y.; Schautz, F.; Dolg, M. *J. Am. Chem. Soc.* **1999**, *121*, 1502–1512. (d) Dolg, M. *J. Chem. Inf. Comput. Sci.* **2001**, *41*, 18–21. (e) Marcalo, J.; de Matos, A. P. *J. Organomet. Chem.* **2002**, *647*, 216–224. (f) Giesbrecht, G. R.; Gordon, J. C.; Clark, D. L.; Hay, P. J.; Scott, B. L.; Tait, C. D. *J. Am. Chem. Soc.* **2004**, *126*, 6387–6401.

(9) Weinhold, F.; Landis, C. In *Valency and Bonding: A Natural Bond Orbital Donor-Acceptor Perspective*; Cambridge University Press: Cambridge, U.K., 2005.

(10) (a) Pepper, M.; Bursten, B. E. *Chem. Rev.* **1991**, *91*, 719–741. (b) Brennan, J. G.; Stults, S. D.; Andersen, R. A.; Zalkin, A. *Organometallics* **1988**, *7*, 1329–1334.

(11) Zhu, Y. J. *Radiochim. Acta* **1995**, *68*, 95–98.

(12) (a) Dohmeier, C.; Robl, C.; Tacke, M.; Schnöckel, H. *Angew. Chem., Int. Ed. Engl.* **1991**, *30*, 564–565. (b) Dohmeier, C.; Loos, D.; Schnöckel, H. *Angew. Chem., Int. Ed. Engl.* **1996**, *35*, 129–149.

(13) (a) Arnold, P. L.; Casely, I. J. *Chem. Rev.* **2009**, *109*, 3599–3611, part of themed issue on carbene chemistry. (b) Maron, L.; Bourissou, D. *Organometallics* **2007**, *26*, 1100–1103.

(14) (a) Jutzi, P.; Schebaum, L. O. *J. Organomet. Chem.* **2002**, *654*, 176–179. (b) Roesky, P. W. *Dalton Trans.* **2009**, 1887–1893.

(15) Huber, M.; Henke, P.; Schnöckel, H. *Chem.—Eur. J.* **2009**, *15*, 12180–12183.

(16) (a) Macdonald, C. L. B.; Cowley, A. H. *J. Am. Chem. Soc.* **1999**, *121*, 12113–12126. (b) Jutzi, P.; Neumann, B.; Reumann, G.; Stammler, H. G. *Organometallics* **1998**, *17*, 1305–1314. (c) Yu, Q.; Purath, A.; Donchev, A.; Schnöckel, H. *J. Organomet. Chem.* **1999**, *584*, 94–97.

(17) (a) Gamer, M. T.; Roesky, P. W.; Konchenko, S. N.; Nava, P.; Ahlrichs, R. *Angew. Chem., Int. Ed.* **2006**, *45*, 4447–4451. (b) Wiecko, M.; Roesky, P. W. *Organometallics* **2007**, *26*, 4846–4848. (c) Liddle, S. T.; Mills, D. P. *Dalton Trans.* **2009**, 5592–5605.

(18) (a) Minasian, S. G.; Krinsky, J. L.; Williams, V. A.; Arnold, J. *J. Am. Chem. Soc.* **2008**, *130*, 11262–11263. (b) Minasian, S. G.; Krinsky, J. L.; Rinehart, J. D.; Copping, R.; Tyliszczak, T.; Janousch, M.; Shuh, D. K.; Arnold, J. *J. Am. Chem. Soc.* **2009**, *131*, 13767–13783.

(19) For selected DFT studies on trivalent Ln and An compounds see: (a) Li, J.; Bursten, B. E. *J. Am. Chem. Soc.* **1998**, *120*, 11456–11466. (b) Vetere, V.; Maldivi, P.; Adamo, C. *J. Comput. Chem.* **2003**, *24*, 850–858. (c) Batista, E. R.; Martin, R. L.; Hay, P. J.; Peralta, J. E.; Scuseria, G. E. *J. Chem. Phys.* **2004**, *121*, 2144–2150. (d) Wang, X. F.; Andrews, L.; Gagliardi, L. *J. Phys. Chem. A* **2008**, *112*, 1754–1761. (e) Yahia, A.; Maron, L. *Organometallics* **2009**, *28*, 672–679. (f) Maron, L.; Eisenstein, O.; Andersen, R. A. *Organometallics* **2009**, *28*, 3629–3635. (g) Elkechai, A.; Boucekkine, A.; Belkhiri, L.; Amarouche, M.; Clappe, C.; Hauchard, D.; Ephritikhine, M. *Dalton Trans.* **2009**, 2843–2849.

(20) (a) Chatterjee, A.; Maslen, E. N.; Watson, K. J. *Acta Crystallogr., Sect. B* **1988**, *44*, 381–386. (b) Gerkin, R. E.; Reppart, W. J. *Acta Crystallogr., Sect. C* **1984**, *40*, 781–786. (c) Matsumoto, K.; Suzuki, K.; Tsukuda, T.; Tsubomura, T. *Inorg. Chem.* **2010**, *49*, 4717–4719. (d) Seitz, M.; Oliver, A. G.; Raymond, K. N. *J. Am. Chem. Soc.* **2007**, *129*, 11153–11160.

dried at 150 °C for at least 12 h, or flame-dried under vacuum prior to use. Toluene and *n*-pentane were purified by passage through a column of activated alumina,[21] stored over sodium/benzophenone, and vacuum transferred immediately prior to use. Deuterated toluene and benzene were vacuum transferred from NaK/benzophenone. NMR spectra were recorded at ambient temperature (unless otherwise indicated) on a Bruker DRX-500 spectrometer. ^{1}H NMR chemical shifts are given relative to residual solvent peaks and coupling constants (J) are given in hertz (Hz). ^{27}Al NMR chemical shifts are referenced to an external standard of 1 M $Al(NO_3)_3$ in H_2O/D_2O (δ 0 ppm). $(Cp^*Al)_4$,[22] Cp*Ga,[14a] and $(CpSiMe_3)_3U$[23] were prepared by the literature procedures, and $(CpSiMe_3)_3Ce$ was synthesized according to a procedure alternative to that previously published[24] (see Supporting Information). Unless otherwise noted, all other reagents were acquired from commercial sources and used as received. X-ray structural determinations were performed at CHEXRAY, University of California, Berkeley.

NMR Spectroscopic Observation of $(CpSiMe_3)_3Ce-AlCp^*$ (1). The following procedure is analogous to the one previously used to observe $(CpSiMe_3)_3Nd-AlCp^*$.[18b] A suspension of powdered $(Cp^*Al)_4$ (6.0 mg, 9.2 μmol) in d_8-toluene (0.25 mL) was added to a solution of $(CpSiMe_3)_3Ce$ (20 mg, 36 μmol) in d_8-toluene (0.25 mL) and sealed under N_2 in a J-Young NMR tube. The presence of unreacted $(CpSiMe_3)_3Ce$ in solution provided a strong blue color which lightened somewhat on heating with the aid of an external heat source. The sample was heated to 82.8 °C inside the probe of a DRX-500 NMR spectrometer, given approximately 30 min to reach equilibrium, and ^{1}H and ^{27}Al NMR spectra were collected. While cooling to −33.2 °C, a spectrum was collected approximately every 10 °C, allowing 15 min at each temperature adjustment for the system to reach equilibrium. ^{1}H NMR (500 MHz, d_8-toluene): the spectra are summarized in the Supporting Information, Table S2. ^{27}Al NMR (130 MHz, d_8-toluene): no signal detected between ±1800 ppm.

NMR Spectroscopic Observation of $(CpSiMe_3)_3Ce-GaCp^*$ (2). A solution of Cp*Ga (n molar equivalents) in d_8-toluene (0.25 mL) was added to a dark blue solution of $(CpSiMe_3)_3Ce$ (20 mg, 36 μmol) in d_8-toluene (0.25 mL) and sealed under N_2 in a J-Young NMR tube. The value of n is chosen to achieve the desired molar fraction (x_{CeGa}) of product in solution; limit behavior is reached above $n = 10$. At room temperature, little or no color change was observed with $n < 10$; however, at $n > 10$ and above the solution became a faint gray color. Cooling solutions with $n > 5$ to −78 °C resulted in a dramatic color change to orange, while rewarming above about −40 °C returned the dark blue color. ^{1}H NMR (500 MHz, d_8-toluene): the spectra are summarized in the Supporting Information, Table S4.

Determination of Thermodynamic Parameters for 2. A standard procedure was followed based on a slight modification of the literature methods.[2b,18b] For example, a solution of $(CpSiMe_3)_3Ce$ (20 mg, 36 μmol) in d_8-toluene (0.25 mL) was combined with a solution of n molar equivalents of Cp*Ga in d_8-toluene (0.25 mL) under N_2 in a J-Young NMR tube. ^{1}H NMR spectra were collected at 10 °C intervals between −33.2 and 19.2 °C, allowing 15 min between steps. Separate samples were prepared for each value of n. The $CpSiMe_3$ resonances were not shifted upon adding additional equivalents of Cp*Ga once limit behavior was reached ($n = 15$). The spectra are summarized in Supporting Information, Table S4, and thermodynamic parameters ΔH and ΔS are given in Supporting Information, Table S5.

Table 1. Molar Fractions (x_{MGa}), Separation Factors ($S_{U/Ce}$),[a] and Speciation Percentages[b] for Formation of $(CpSiMe_3)_3U-GaCp^*$ or $(CpSiMe_3)_3Ce-GaCp^*$ during ^{1}H NMR Competition Reactions

T (°C)	x_{UGa}	x_{CeGa}	$S_{U/Ce}$	% U−Ga	% Ce−Ga
−33	0.79(1)	0.061(3)	13.0(5)	92.8(2)	7.2(2)
−22	0.72(1)	0.054(3)	13.2(6)	93.0(3)	7.0(3)
−11	0.64(2)	0.046(3)	13.8(7)	93.2(3)	6.8(3)
−1.6	0.55(2)	0.040(4)	13.8(8)	93.2(4)	6.8(4)
8.9	0.46(2)	0.035(4)	13.3(8)	93.0(4)	7.0(4)
19	0.38(2)	0.030(4)	12.6(8)	92.6(4)	7.4(4)

[a] $S_{U/Ce} = x_{UGa}/x_{CeGa}$. [b] Percentage of the total formation of either product, calculated by setting $x_{UGa} + x_{CeGa} = 1$, such that specation % $= x_{MGa}/(x_{UGa} + x_{CeGa})$.

Competition Reactions. The literature procedure[2b,18b] was followed: a solution of $(CpSiMe_3)_3U-GaCp^*$ (20 mg, 23 μmol) in d_8-toluene (0.25 mL) was combined with a solution of $(CpSiMe_3)_3Ce$ (13 mg, 23 μmol) in d_8-toluene (0.25 mL) under N_2 in a J-Young NMR tube. After at least 10 min, a ^{1}H NMR spectrum was collected. The experiment was repeated five times on independent samples, and results are summarized in Table 1. Samples were prepared in a similar fashion for the Al system, and relative concentrations were determined by integration of the peaks corresponding to the independent Cp* proton resonances in $(CpSiMe_3)_3U-AlCp^*$ and $(CpSiMe_3)_3Ce-AlCp^*$. Monomeric Cp*Al does not persist in detectable concentrations at room temperature;[12b] therefore we assume the intensity of these peaks derives entirely from the presence of $(CpSiMe_3)_3U-AlCp^*$ or $(CpSiMe_3)_3Ce-AlCp^*$.

Computational Methods. All structures and energies were calculated using the Gaussian09 suite of programs.[25] Self-consistent field computations were performed with tight convergence criteria on ultrafine grids, while geometry optimizations were converged to tight geometric convergence criteria for all compounds $Cp_3Ln-ECp$, Cp_3Ln, and CpE. In some instances it was necessary to use the quadratic convergence method to achieve SCF convergence.[26] All lanthanide complexes were modeled with the unrestricted formalism, except those containing La and Lu, and were assumed to be in their highest-spin state (except the Nd and Gd compounds for which all plausible multiplicities were investigated). Spin expectation values $\langle S^2 \rangle$ indicated that spin contamination was not significant in any result. The use of symmetry was explicitly turned off for all computations. Frequencies were calculated analytically at 298.15 K and 1 atm. Structures were considered true minima if they did not exhibit imaginary modes with frequencies greater than $15i$ cm^{-1}, and in cases where one of these vibrations was allowed it was confirmed to correspond with one of the six formally zero-valued molecular translational/rotational modes. Electronic stability calculations were performed on all Ln species, and in those cases where an orbital instability was found this instability was corrected and the molecular geometry reoptimized. This process was repeated until a well-converged, electronically stable structure was obtained.

The hybrid B3PW91[27] functional was used throughout because of its satisfactory performance in our previous work. Stuttgart-type small core ECPs and their appropriate valence basis sets were used for Ga[28] and the lanthanides,[29] with

(21) Alaimo, P. J.; Peters, D. W.; Arnold, J.; Bergman, R. G. *J. Chem. Educ.* **2001**, *78*, 64–64.
(22) Schormann, M.; Klimek, K. S.; Hatop, H.; Varkey, S. P.; Roesky, H. W.; Lehmann, C.; Röpken, C.; Herbst-Irmer, R.; Noltemeyer, M. *J. Solid State Chem.* **2001**, *162*, 225–236.
(23) Brennan, J. G.; Andersen, R. A.; Zalkin, A. *Inorg. Chem.* **1986**, *25*, 1756–1760.
(24) Stults, S. D.; Andersen, R. A.; Zalkin, A. *Organometallics* **1990**, *9*, 115–122.
(25) Frisch, M. J., et al. *Gaussian09*, revision A.2; Gaussian, Inc.: Wallingford, CT, 2009. Complete citation in the Supporting Information.
(26) Bacskay, G. B. *Chem. Phys.* **1981**, *61*, 385–404.
(27) (a) Becke, A. D. *Phys. Rev. A* **1988**, *38*, 3098–3100. (b) Perdew, J. P. In *Electronic Structure of Solids*; Ziesche, P., Esching, H., Eds.; Akademie Verlag: Berlin, 1991. (c) Becke, A. D. *J. Chem. Phys.* **1993**, *98*, 5648–5652.
(28) (a) Metz, B.; Stoll, H.; Dolg, M. *J. Chem. Phys.* **2000**, *113*, 2563–2569. (b) Peterson, K. A. *J. Chem. Phys.* **2003**, *119*, 11099–11112.
(29) (a) Dolg, M.; Stoll, H.; Preuss, H. *J. Chem. Phys.* **1989**, *90*, 1730–1734. (b) Cao, X. Y.; Dolg, M. *J. Mol. Struct.* (*THEOCHEM*) **2002**, *581*, 139–147.

valence contraction schemes (11s12p10d2f)/[6s5p4d2f] and segmented (14s13p10d8f6g)/[10s9p5d4f3g], respectively. Note that the valence bases used were those taken from their Web site[30] rather than those included in the Gaussian code. For geometry optimizations, frequency calculations, and electronic stability calculations, the remaining atoms were treated with Pople's 6-31G(d) double-ζ split-valence basis[31] except for Al and O (and Ga, see above) which were treated with the triple-ζ 6-311+G(d) basis.[32] No polarization functions were added for H. This combination is referred to here as BS1.

Single point energy calculations were performed on all optimized structures wherein all atoms not using ECPs were treated with the 6-311+G(d,p) basis (referred to as BS2), and the zero point energies calculated at BS1 were added to those to obtain 0 K Ln−E heterolytic bond disruption enthalpies (*BDEs*). These values are essentially $\Delta H_{rxn,0K}$ for the gas-phase ligand dissociation reaction. In cases of difficult SCF convergence at BS2, electronic stability calculations were repeated at this basis. Scaled *BDE*s were obtained by adding 0.9 kcal mol^{-1} to the calculated enthalpies, a correction which was derived by averaging the error for the model complexes $Cp_3M-GaCp$ (M = Nd, U), with respect to the average of the experimentally determined values for the fully substituted $(CpSiMe_3)_3M-GaCp^*$ adducts. Because of this empirical fitting scheme, it was deemed inappropriate to apply corrections for basis set superposition error (BSSE). Ligand reorganization energies (*LRE*) were obtained by performing additional single-point energy calculations on the Cp_3Ln and CpAl fragments at their adduct geometries for each $Cp_3Ln-AlCp$ species, using BS2.

Natural population analyses (NPA), natural bond orbital (NBO), and natural localized molecular orbital (NLMO)[33] analyses were performed as follows: NBO archive files were generated by Gaussian's built-in NBO3.1.[34] These files were then used as input for a modified version of the stand-alone GENNBO5.0[35] in which the lanthanide 5d subshells were included in the valence space.[36] The NBO keyword combination *bndidx*, *dipole*, and *cmo*, as well as the standard NBO output, yielded all of the NBO/NLMO data presented here. Tabulated values for those data presented in plots are available in the Supporting Information.

Results and Discussion

1. Experimental Observation of Cerium Complexes. We have previously described the synthesis and characterization of $(CpSiMe_3)_3M-ECp^*$ (M = Nd, U; E = Al, Ga).[18b] Both U complexes were isolated as pure crystalline solids and characterized by standard techniques; the Nd complexes were observed only by NMR spectroscopy. The isostructural and isoelectronic $4f^3/5f^3$ system was chosen to ensure that any observed differences in the electronic structure were not due to a difference in electron configuration. However, the Nd atom in $(CpSiMe_3)_3Nd$ is slightly smaller than the U atom in $(CpSiMe_3)_3U$ (Nd−C average distance = 2.76 Å; U−C average distance = 2.78 Å), and so $(CpSiMe_3)_3Ce$ was prepared as a more suitable Ln analogue to $(CpSiMe_3)_3U$ on steric grounds. A crystal structure was obtained (see Supporting Information), revealing a Ce environment which is slightly less congested than that in $(CpSiMe_3)_3U$ (Ce−C average distance = 2.80 Å).

Combining equivalent amounts of $(CpSiMe_3)_3Ce$ and $(Cp^*Al)_4$ or Cp*Ga in solution at ambient temperature did not result in a discernible color change from the characteristic deep blue color of $(CpSiMe_3)_3Ce$. However, in the presence of $(Cp^*Al)_4$ in d_8-toluene, the color lightened somewhat upon gentle heating. Additionally, the anticipated peak corresponding to monomeric Cp*Al (δ −150 ppm)[12,37] in the ^{27}Al NMR spectrum of a $(CpSiMe_3)_3Ce/(Cp^*Al)_4$ mixture was not observed at about 50 °C, suggesting that all free Cp*Al was coordinated to a paramagnetic species. A pentane solution of $(CpSiMe_3)_3Ce$ containing excess Cp*Ga (ca. 10 equiv) was pale blue-gray in color, and became red-orange upon cooling to −78 °C. The color-change was reversible: the blue-gray color returned upon warming above about −70 °C. This behavior is consistent with our earlier work on the Nd analogue, and similar colors have been observed for related $(CpSiMe_3)_3Ce$ complexes with azine ligands.[2b]

Despite considerable synthetic effort, no crystalline products from these reactions could be obtained either from pure solutions or in the presence of co-crystallizing agents. These observations are again consistent with our previous studies on the analogous Nd adducts, which suggest that formation of $(CpSiMe_3)_3Ce-AlCp^*$ (**1**) occurs at elevated temperatures, while $(CpSiMe_3)_3Ce-GaCp^*$ (**2**) exists only in the presence of excess Cp*Ga or at low temperatures (eq 1). To the best of our knowledge this is the first reported evidence of complexes containing cerium−metal bonds.

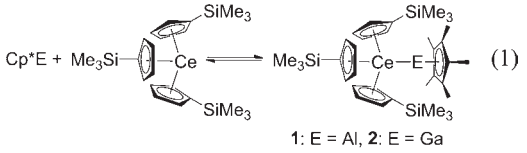

2. Determination of Thermodynamic Parameters. Ephritikhine and co-workers have previously outlined how ^{1}H NMR titration may be used to determine thermodynamic parameters for systems undergoing fast ligand exchange on the NMR time scale.[2b] This method was successfully employed for the $(CpSiMe_3)_3M-GaCp^*$ (M = Nd, U) system, but could not be used for the Al complexes because $(Cp^*Al)_4$ aggregates and is prone to crystallization, forming heterogeneous mixtures.

Limit behavior, obtained for a solution of mostly **2** and virtually no $(CpSiMe_3)_3Ce$ starting material, was achieved with $n > 20$ equiv of Cp*Ga. The derived ambient-temperature equilibrium constant (K_{CeGa} = 1.460(1)) indicates that formation of **2** is energetically comparable to that of $(CpSiMe_3)_3Nd-GaCp^*$ (K_{NdGa} = 2.0(1)), but both are considerably less favorable than formation of $(CpSiMe_3)_3U-GaCp^*$ (K_{UGa} = 21.4(2)). A van't Hoff analysis was performed, affording thermodynamic parameters ΔH_{CeGa} (−4.2(1) kcal mol^{-1}) and ΔS_{CeGa} (−12(1) cal mol^{-1} K^{-1}).

(30) Institut für Theoretische Chemie, Stuttgart/Cologne group. http://www.theochem.uni-stuttgart.de/psuedopotentials/ (accessed Aug 15, 2010).
(31) (a) Hehre, W. J.; Ditchfield, R.; Pople, J. A. *J. Chem. Phys.* **1972**, *56*, 2257. (b) Hariharan, P. C.; Pople, J. A. *Theor. Chim. Acta* **1973**, *28*, 213.
(32) (a) Krishnan, R.; Binkley, J. S.; Seeger, R.; Pople, J. A. *J. Chem. Phys.* **1980**, *72*, 650–654. (b) McLean, A. D.; Chandler, G. S. *J. Chem. Phys.* **1980**, *72*, 5639–5648.
(33) (a) Reed, A. E.; Weinhold, F. *J. Chem. Phys.* **1985**, *83*, 1736–1740. (b) Hübler, K.; Hunt, P. A.; Maddock, S. M.; Rickard, C. E. F.; Roper, W. R.; Salter, D. M.; Schwerdtfeger, P. *Organometallics* **1997**, *16*, 5076–5083.
(34) Reed, A. E.; Curtiss, L. A.; Weinhold, F. *Chem. Rev.* **1988**, *88*, 899–926.
(35) Glendening, E. D.; Badenhoop, J. K.; Reed, A. E.; Carpenter, J. E.; Bohmann, J. A.; Morales, C. M.; Weinhold, F. *NBO 5.0*; http://www.chem.wisc.edu/~nbo5 (accessed Aug 15, 2010).
(36) Clark, A. E. *J. Chem. Theory Comput.* **2008**, *4*, 708–718.
(37) Gauss, J.; Schneider, U.; Ahlrichs, R.; Dohmeier, C.; Schnöckel, H. *J. Am. Chem. Soc.* **1993**, *115*, 2402–2408.

These values indicate that formation of the Ce−Ga bond is slightly more favorable than formation of the related Nd−Ga bond (ΔH_{NdGa} (−3.0(2) kcal mol^{-1}), ΔS_{NdGa} (−9.1(7) cal mol^{-1} K^{-1})), yet still disfavored relative to formation of a U−Ga bond (ΔH_{UGa} (−5.8(2) kcal mol^{-1}), ΔS_{UGa} (−13.4(6) cal mol^{-1} K^{-1})).

Competition reactions between $(CpSiMe_3)_3Ce$ and $(CpSiMe_3)_3U$ for Cp*Ga were also monitored by ^{1}H NMR spectroscopy, using the method previously discussed.[18b] Both the U−Ga and Ce−Ga adducts were formed upon addition of 1 equiv of Cp*Ga (relative to Ce or U) to a 1:1 mixture of $(CpSiMe_3)_3Ce$ and $(CpSiMe_3)_3U$ in d_8-toluene. The molar fractions of each product (x_{MGa}), separation factors ($S_{U/Ce}$), and speciation percentages (summed to unity) are listed in Table 1. In contrast to the U/Nd competition results, in this U/Ce system the separation factors remain almost identical between −33 and 19 °C, presumably because of a better entropy match for the formation of U and Ce complexes. The 5f/4f selectivity at low temperature is diminished somewhat relative to the U/Nd system ($S_{U/Nd}$ = 23.2(5) at −33 °C), but is identical at ambient temperature ($S_{U/Nd}$ = 13.9(2) at 19 °C) and remains excellent relative to other known examples where the examination of selectivity arising from interactions with soft, single donor-atom ligands was explored.[2b,c]

Because of the heterogeneity of $(Cp^*Al)_4$ solutions, no quantitative competition measurements could be made for the formation of Al complexes; however, some qualitative comments can be made. A sample containing 1/4$(Cp^*Al)_4$ and a 1:1 mixture of $(CpSiMe_3)_3U$ and $(CpSiMe_3)_3Ce$ in d_8-toluene contained only trace **2**, while the concentration of $(CpSiMe_3)_3U-AlCp^*$ was not detectably reduced, on the basis of peak intensities. We have previously noted that this excellent selectivity could be expected if the U−Al interaction is favorable, and Ln−Al interaction (Ln = Nd, Ce) is unfavorable, relative to the tetramerization of Cp*Al (9(1) kcal mol^{-1}).[12] Therefore, this hypothesis suggests that Cp*Al is an unusual example of a ligand approaching ideal An/Ln selectivity.

3. Trends in Metal−Ligand Bond Lengths. We begin our discussion of computational results with an analysis of geometrical parameters because these are most straightforwardly compared with available experimental data for similar compounds. The reader is cautioned that experimental trends in the more weakly binding adducts can be obscured by crystal packing forces because of their shallow or soft potential energy surfaces, and thus agreement between computed bonding parameters and those taken from solid-state X-ray data can be inherently poor regardless of the computational methodology used. Additionally, as stated in the Experimental Details, lanthanide-containing species were generally assumed to be in their highest-multiplicity spin states. Electronic states of lower multiplicity may be important in a multiconfigurational treatment of some complexes and thus the use of a single-determinantal (and hybrid) DFT method here may complicate the comparison of different Ln centers across the period where static correlation is of differing importance.[38] The computed average

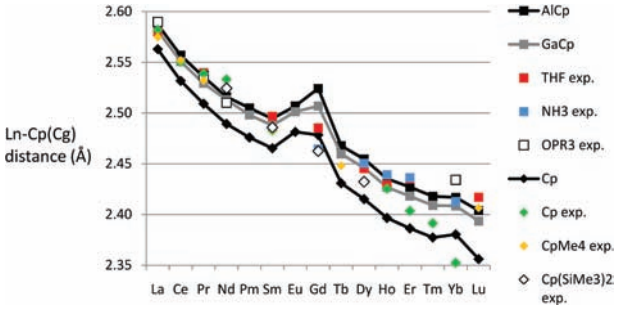

Figure 1. Ln−Cp(centroid) distances (Å) in Cp_3Ln complexes: squares indicate Cp_3Ln-L and are labeled by L; diamonds indicate $(CpR_x)_3Ln$ and are labeled by Cp substitution. Experimental values are taken from crystallographic data.

Ln−Cp(Cg) (Cg = centroid) distances in $Cp_3Ln-ECp$ and Cp_3Ln are presented in Figure 1, accompanied by experimental solid-state data for those series having at least four known lanthanide analogues.[39] In Figure 1 those data points represented with squares correspond to average d(Ln−Cp(Cg)) values in Cp_3Ln-L adducts and are labeled according to the identity of L, whereas those represented by diamonds correspond to the base-free

(38) (a) Tschinke, V.; Ziegler, T. *J. Chem. Phys.* **1990**, *93*, 8051–8060. (b) Schultz, N. E.; Zhao, Y.; Truhlar, D. G. *J. Phys. Chem. A* **2005**, *109*, 4388–4403. (c) Schultz, N. E.; Zhao, Y.; Truhlar, D. G. *J. Phys. Chem. A* **2005**, *109*, 11127–11143. (d) Furche, F.; Perdew, J. P. *J. Chem. Phys.* **2006**, *124*, 044103.

(39) Arranged according to X_3Ln-L: (a) [Ln = La; X = Cp; L = THF] Rogers, R. D.; Atwood, J. L.; Emad, A.; Sikora, D. J.; Rausch, M. D. *J. Organomet. Chem.* **1981**, *216*, 383–392. (b) [Ln = Pr; X = Cp; L = THF] Junk, P. C. *Appl. Organomet. Chem.* **2003**, *17*, 875–876. (c) [Ln = Nd; X = Cp; L = THF] Benetollo, F.; Bombieri, G.; Castellani, C. B.; Jahn, W.; Fischer, R. D. *Inorg. Chim. Acta* **1984**, *95*, L7–L10. (d) [Ln = Sm; X = Cp; L = THF] Gunko, Y. K.; Belskii, V. K.; Soloveichik, G. L.; Bulychev, B. M. *Russ. Chem. Bull.* **1993**, *42*, 1086–1089. (e) [Ln = Sm, Dy; X = Cp; L = THF] Wu, Z.; Xu, Z.; You, X.; Zhou, X.; Huang, X.; Chen, J. *Polyhedron* **1994**, *13*, 379–384. (f) [Ln = Gd; X = Cp; L = THF] Rogers, R. D.; Vannbynum, R.; Atwood, J. L. *J. Organomet. Chem.* **1980**, *192*, 65–73. (g) [Ln = Ho; X = Cp; L = THF] Zaeni, A.; Edelmann, F. T.; Kaehler, T.; Olbrich, F. Data for this structure are deposited with the Cambridge Structural Database as deposition number 178657. (h) [Ln = Er; X = Cp; L = THF] Chen, W. Q.; Lin, G. Y.; Xia, J. S.; Wei, G. C.; Zhang, Y.; Jin, Z. S. *Acta Chim. Sin.* **1994**, *52*, 261–267. (i) [Ln = Lu; X = Cp; L = THF] Chaozhou, N.; Daoli, D.; Changtao, Q. *Inorg. Chim. Acta* **1985**, *110*, L7–L10. (j) [Ln = Gd, Dy, Ho, Er; X = Cp; L = NH_3] Baisch, U.; Zeuner, M.; Barros, N.; Maron, L.; Schnick, W. *Chem.—Eur. J.* **2006**, *12*, 4785–4798. (k) [Ln = Yb; X = Cp; L = NH_3] Baisch, U.; Pagano, S.; Zeuner, M.; Schnick, W. *Eur. J. Inorg. Chem.* **2006**, 3517–3524. (l) [Ln = La, Pr; X = Cp; L = OPR_3] Amberger, H. D.; Zhang, L. X.; Reddmann, H.; Apostolidis, C.; Walter, O. *Z. Anorg. Allg. Chem.* **2006**, *632*, 2467–2470. (m) [Ln = Nd, Yb; X = Cp; L = OPR_3] Deacon, G. B.; Fallon, G. D.; Forsyth, C. M.; Gatehouse, B. M.; Junk, P. C.; Philosof, A.; White, P. A. *J. Organomet. Chem.* **1998**, *565*, 201–210. (n) [Ln = La; X = Cp; L = None] Rebizant, J.; Apostolidis, C.; Spirlet, M. R.; Kanellakopulos, B. *Acta Crystallogr., Sect. C* **1988**, *44*, 614–616. (o) [Ln = Ce, Ho; X = Cp; L = None] Baisch, U.; Pagano, S.; Zeuner, M.; Gunne, J.; Oeckler, O.; Schnick, W. *Organometallics* **2006**, *25*, 3027–3033. (p) [Ln = Pr; X = Cp; L = None] Hinrichs, W.; Melzer, D.; Rehwoldt, M.; Jahn, W.; Fischer, R. D. *J. Organomet. Chem.* **1983**, *251*, 299–305. (q) [Ln = Nd; X = Cp; L = None] Eggers, S.; Hinrichs, W.; Kopf, J.; Fischer, R. D.; Xing-Fu, L. Data for this structure are deposited with the Cambridge Structural Database as deposition number 51485. (r) [Ln = Sm; X = Cp; L = None] Laubereau, P. G.; Burns, J. H. *Inorg. Chem.* **1970**, *9*, 1091–1095. (s) [Ln = Er, Tm; X = Cp; L = None] Eggers, S. H.; Hinrichs, W.; Kopf, J.; Jahn, W.; Fischer, R. D. *J. Organomet. Chem.* **1986**, *311*, 313–323. (t) [Ln = Yb; X = Cp; L = None] Eggers, S. H.; Kopf, J.; Fischer, R. D. *Acta Crystallogr., Sect. C* **1987**, *43*, 2288–2290. (u) [Ln = Lu; X = Cp; L = None] Eggers, S. H.; Schultze, H.; Kopf, J.; Fischer, R. D. *Angew. Chem., Int. Ed. Engl.* **1986**, *25*, 656–657. (v) [Ln = La, Sm; X = $CpMe_4$; L = None] Schumann, H.; Glanz, M.; Hemling, H.; Hahn, F. E. *Z. Anorg. Allg. Chem.* **1995**, *621*, 341–345. (w) [Ln = Ce, Pr; X = $CpMe_4$; L = None] Evans, W. J.; Rego, D. B.; Ziller, J. W. *Inorg. Chem.* **2006**, *45*, 10790–10798. (x) [Ln = Tb; X = $CpMe_4$; L = None] Schumann, H.; Glanz, M.; Hemling, H. *J. Organomet. Chem.* **1993**, *445*, C1–C3. (y) [Ln = Lu; X = $CpMe_4$; L = None] Evans, W. J.; Lee, D. S.; Johnston, M. A.; Ziller, J. W. *Organometallics* **2005**, *24*, 6393–6397. (z) [Ln = La, Nd, Gd, Dy; X = $Cp(SiMe_3)_2$; L = None] Xie, Z. W.; Chui, K. L.; Liu, Z. X.; Xue, F.; Zhang, Z. Y.; Mak, T. C. W.; Sun, J. *J. Organomet. Chem.* **1997**, *549*, 239–244. (aa) [Ln = Sm; X = $Cp(SiMe_3)_2$; L = None] Evans, W. J.; Keyer, R. A.; Ziller, J. W. *J. Organomet. Chem.* **1990**, *394*, 87–97.

compounds $(CpR_x)_3Ln$ and are labeled by differing Cp substitution.

In general the d(Ln−Cp(Cg)) values decrease smoothly, with some attenuation which is expected because of the quadratic nature of the lanthanide contraction and interligand steric clashes.[20d,40] All values fall in a narrow range for each lanthanide element regardless of the presence or absence of a dative ligand, highlighting the dominant role of the relatively strong Cp−Ln bond in these systems. An exception is the trend in values for the unsubstituted Cp_3Ln complexes (although strong intermolecular interactions present in the solid-state structures of the erbium, thulium, and ytterbium analogues render those three values unreliable[39s,t]). The usable solid-state Cp_3Ln values are significantly larger than those calculated here, and so the current method should be assumed to underestimate the Cp−Ln bond distances in this case. That being stated, the Cp−Ln distances calculated for Cp_3Ln−ECp closely match the experimental values reported for both the base-free and the ligated Cp_3Ln derivatives.

Deviations from the trend in calculated Ln−Cp(Cg) distances include a local increase at europium, gadolinium, and ytterbium for the CpE adducts as well as the base-free Cp_3Ln species. Few experimental data are available for these elements; the Cp_3Gd−THF (THF = tetrahydrofuran) adduct[39f] may display this behavior to some degree, but it is unclear if it is observed in any other analogous system. This local expansion may be related to ligand field effects, as a similar behavior was noted for the crystal field strengths of Ln^{3+} in $LaCl_3$;[41] however, we must currently regard the prediction of this phenomenon as suspect. Because this anomaly is consistent between the CpE adducts and the free Cp_3Ln fragments we assume that the principal role it will play in determining the Ln−E bonding trends will be that slightly more room is available around the Ln center in these cases than in their neighboring analogues and thus some Ln−E overbinding may be expected.

It was not known a priori what effect orbital interactions might have on the Ln−E bond lengths. We found that the computed d(Ln−E) values do decrease across the period as expected, although within each half period the values level off and a large increase is observed at Eu and Yb (Figure 2). This contrasts sharply with the monotonically decreasing experimental and calculated values of d(Ln−O) in $Ln(H_2O)_{8,9}^{3+}$, the latter using similar methods as here.[1h] From the available experimental data it appears that a monotonic trend is also observed for d(Ln−O) in Cp_3Ln−THF[39a−i] (plotted against the secondary axis in Figure 2) but unfortunately no values exist for the Eu or Yb adducts. To help address this issue, the predicted geometries of all Cp_3Ln−THF adducts were calculated, and the resulting d(Ln−O) values plotted with the experimental data against the secondary axis in Figure 2. The bond lengths are overestimated by about 0.13 Å in general, and increase at Eu/Yb (and less so at Sm/Tm) like those in the CpE adducts. These deviations, however, are much less pronounced in the THF adducts

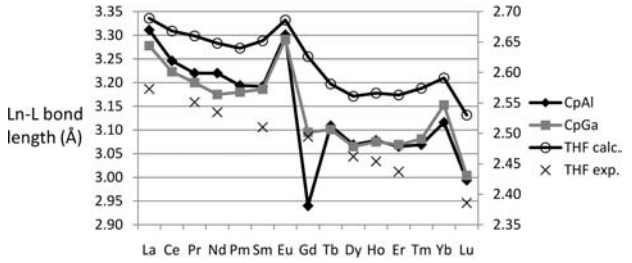

Figure 2. Calculated Ln−L bond lengths d(Ln−E, O) (Å) in Cp_3Ln−ECp (E = Al, Ga) and Cp_3Ln−THF. Experimentally determined and calculated d(Ln−O) values for Cp_3Ln−THF are plotted against the secondary axis.

than those of CpE. In light of these data it must be suspected that the corresponding deviations in d(Ln−E) values for Cp_3Ln−ECp are at least partially an artifact of the computational method and thus some underestimation (relative to the series) of the Eu/Yb−E bonding interaction might be expected (but recall that the anomalously long d(Eu/Yb−Cp(Cg)) values suggest the opposite). We note that, in this model system, upon moving across the lanthanide row it is at Eu and Yb that the f_σ orbital (aligned along the Ln−E bond) is newly populated.[42] That the deviations are greater for the CpE ligands than for THF suggests that this repulsive Ln(core)-ligand(lone-pair) electronic effect, while possibly exaggerated computationally, has a stronger influence on a labile ligand such as CpE. Unfortunately sufficient experimental data for very weakly binding ligands are not available to support or contradict these findings.

In contrast to d(Ln−Cp(Cg)), the total bond length contraction between lanthanum and lutetium (0.317 and 0.274 Å for the CpAl and CpGa series, respectively) far exceeds the experimentally determined representative value of about 0.18 Å for the lanthanide contraction[6a,43] (the experimental and calculated values for the Cp_3Ln−THF adducts are 0.187 and 0.159 Å, respectively), which is consistent with the proposal that the lanthanide contraction is more pronounced for soft ligands.[40a] The computed Gd−E bond lengths are smaller than those of the next Ln ion of the row (Tb), with Cp_3Gd−AlCp displaying a distance much smaller than even the Lu analogue. This large deviation manifests in all properties of Cp_3Gd−AlCp reported here, and the fact that the deviation is not observed for the CpGa analogue leads one to suspect that it is an erroneous result. This is puzzling because, excluding the closed-shell La and Lu adducts, the Gd species with their half-filled f shells would be expected to be the most amenable to treatment with DFT. Peculiarities were also observed in the calculated Gd−O bond lengths and hydration energies of Gd^{3+} but were rationalized on physical grounds;[1h] however, a deficiency in the method cannot be ruled out. As such, many of the data for the Gd adducts will be omitted from the following discussion, except in section 7. To summarize, examination of geometrical

(40) (a) Schwarz, W. H. E. *Phys. Scr.* **1987**, *36*, 403–411. (b) Quadrelli, E. A. *Inorg. Chem.* **2002**, *41*, 167–169.

(41) (a) Edelstein, N. M. *J. Alloy. Compd.* **1995**, *223*, 197–203. (b) Amberger, H. D.; Reddmann, H.; Mueller, T. J.; Evans, W. J. *Organometallics* **2010**, *29*, 1368–1373.

(42) The f-electron configuration may affect the molecular geometry, see: Groen, C. P.; Varga, Z.; Kolonits, M.; Peterson, K. A.; Hargittai, M. *Inorg. Chem.* **2009**, *48*, 4143–4153.

(43) (a) Krasnov, K. S.; Giricheva, N. I.; Girichev, G. V. *J. Struct. Chem.* **1976**, *17*, 575–577. (b) Shannon, R. D. *Acta Crystallogr., Sect. A* **1976**, *32*, 751–767. (c) Lobanov, N. N.; Venskovskii, N. U. *Russ. J. Inorg. Chem.* **2008**, *53*, 890–896. (d) Lundberg, D.; Persson, I.; Eriksson, L.; D'Angelo, P.; De Panfilis, S. *Inorg. Chem.* **2010**, *49*, 4420–4432.

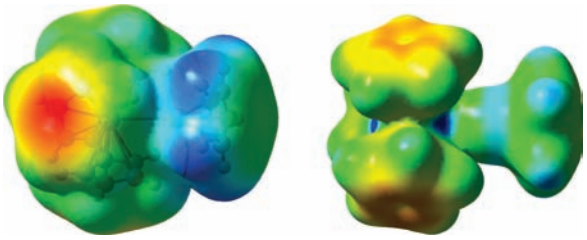

Figure 3. Electrostatic potential projected on the total electron density (isovalue 0.0004 and 0.008, left and right sides respectively) for $Cp_3La-AlCp$. Red is most negative, and blue is most positive.

parameters has highlighted some methodological pitfalls which should be considered during the following analyses. Particularly, all bond distances involving Eu and Yb ions are too large relative to the rest of the series; the anomalous *d*(Ln−Cp(Cg)) and *d*(Ln−E) values may or may not lead to a cancellation of error in thermodynamic properties.

4. Electrostatic and Dipole Effects. The molecular dipole moment might be considered a simple measure of relative electrostatic interaction strength when the dipole is oriented along the bond of interest, which is the case in $Cp_3Ln-ECp$. The electronegativity (*EN*) of the lanthanides increases across the period (monotonically by most derivations),[44] and thus in the case of Cp_3Ln, upon progressing from La^{3+} to Lu^{3+} the Ln ion should retain more electron density formally located on the Cp^- anions. If one assumes that the CpE fragments possess a greater effective electronegativity than the Ln^{3+} ion and that Ln−E bonding is *solely* electrostatic in nature, then one would predict a decrease in the dipole moment in the adducts of the later lanthanides, and thus a decrease in bond strength.

The calculated molecular dipole moments of the CpE adducts indicate that this simple model is deficient in explaining the Ln−E bonding interaction. In fact, the concentration of three Cp^- anions on the Cp_3Ln fragment results in a molecular dipole vector pointing at the CpE fragment (in the direction of positive charge, see Figure 3, left-hand side, $Cp_3La-AlCp$) in all cases. However, upon closer inspection the partial charge at the Ln center is greater than that at the E cation, as illustrated in the right-hand side of Figure 3.

On what, then, do the molecular dipole moments depend, and what is their significance? Figure 4 depicts the computed molecular dipole moments of the model CpE adducts. It is observed that, rather than follow a monotonic trend according to lanthanide *EN* values, the trend in dipole values exhibits a saw-tooth shape wherein the dipole decreases across each half period and then spikes. Xue and co-workers recently proposed a new *EN* scale incorporating pronounced decreases at Gd and Lu.[45] According to this new scale only Tm and Yb surpass Eu in the magnitude of their *EN* values; however, this proposal has met with at least some criticism.[46]

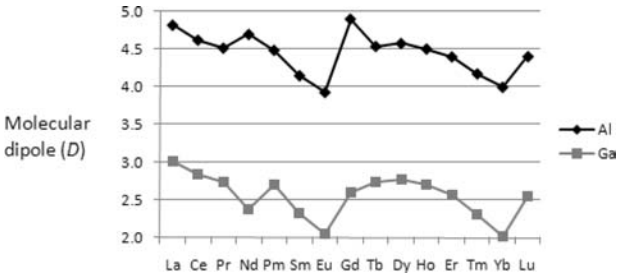

Figure 4. Calculated molecular dipole moments (Debye) in $Cp_3Ln-ECp$, where E = Al, Ga. The dipole vectors are aligned along the Ln−E bond and are directed at the CpE fragment.

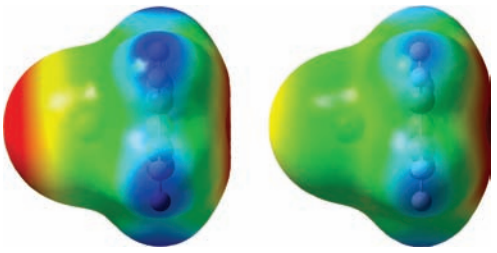

Figure 5. Electrostatic potential projected on the total electron density (isovalue 0.0004) for CpAl (left) and CpGa (right). Red is most negative, and blue is most positive.

Interestingly, this saw-toothed pattern was also reported for the *BDE*s of the zero-valent lanthanide bis(arene) adducts mentioned in the introduction,[8b] which were found to correlate inversely with the f→d promotion energies for the lanthanide atoms and ions.[47] We propose that in this case a larger molecular dipole correlates with a larger Ln−E *BDE* value, which in turn is the result of a stronger CpE ligand-to-metal charge transfer interaction (see section 6) and not a difference in electrostatic contributions to bonding. Further support for this proposal is presented in the following sections.

The calculated dipole moments in the CpGa adducts are roughly half as large as in their aluminum analogues, which can be easily explained on the basis of the electronic distribution in the CpE fragments. In the accepted *EN* scale gallium is slightly more electronegative than aluminum.[16a] However, the *effective EN* of the E^+ cation changes upon interacting with the Cp ligand. As shown in Figure 5, there is significantly more negative charge buildup in the lone-pair region of CpAl than in that of CpGa although the *nucleus*-centered natural charge at Al (0.581) is slightly larger than that at Ga (0.560). Consequentially, more of the electronic charge native to the CpAl moiety is located near the Cp_3Ln fragment, and thus the molecular dipole is enhanced. An alternative and in some ways equivalent explanation is that the Al lone pair is effectively more electron-donating than that of CpGa (the calculated lone-pair orbital energy is −5.90 eV in CpAl and −6.97 eV in CpGa) so that charge transfer to the lanthanide ion is more favorable for the former than for the latter (see section 6).

(44) (a) Sanderson, R. T. *Inorg. Chem.* **1986**, *25*, 1856–1858. (b) Sanderson, R. T. *Inorg. Chem.* **1986**, *25*, 3518–3522. (c) Zhang, Y. G. *Inorg. Chem.* **1982**, *21*, 3886–3889. (d) Martynov, I. V. *Russ. J. Inorg. Chem.* **2008**, *53*, 579–582. (e) Jeong, N. C.; Lee, J. S.; Tae, E. L.; Lee, Y. J.; Yoon, K. B. *Angew. Chem., Int. Ed.* **2008**, *47*, 10128–10132.

(45) (a) Xue, D. F.; Zuo, S.; Ratajczak, H. *Physica B* **2004**, *352*, 99–104. (b) Li, K. Y.; Xue, D. F. *J. Phys. Chem. A* **2006**, *110*, 11332–11337. (c) Li, K. Y.; Xue, D. F. *Phys. Status Solidi B* **2007**, *244*, 1982–1987.

(46) Brown, I. D. *Chem. Rev.* **2009**, *109*, 6858–6919.

(47) (a) Martin, W. C.; Zalubas, R.; Hagan, L. *Atomic Energy Levels - The Rare Earth Elements*; NSRDS-NBS 60; U.S. Department of Commerce: Washington, DC, 1978. (b) Brewer, L. *J. Opt. Soc. Am.* **1971**, *61*, 1101. (c) Brewer, L. *J. Opt. Soc. Am.* **1971**, *61*, 1666–1682.

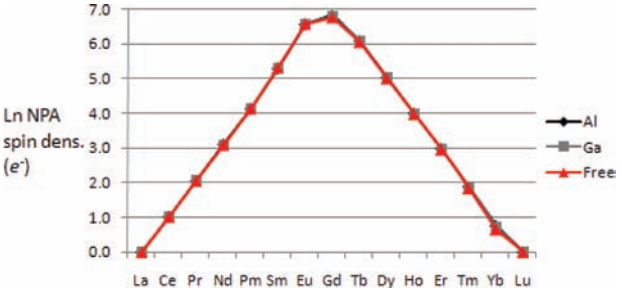

Figure 6. Ln-centered NPA spin densities in $Cp_3Ln-ECp$ (E = Al, Ga) and Cp_3Ln (Free), effective number of unpaired electrons.

5. Lanthanide Electronic Configurations and Spin Densities. Any covalent interactions between the Cp_3Ln fragment and CpE ligand should be of the charge transfer type, where the ligand lone-pair orbital effectively donates some of its electron population to an unoccupied orbital on the acceptor. It has previously been established that Ln→E π-electron donation is not at all significant in these systems; that is, the CpE ligands are pure σ-donors.[18b] Before examining the electronic structure of the lanthanide centers in detail, it is pertinent to first ascertain the overall spin properties of the Ln ions in Cp_3Ln and their CpE adducts. The Ln-centered NPA spin density values for all calculated species are charted in Figure 6. That the spin density values are virtually identical in both adducts as well as base-free Cp_3Ln illustrates the CpE ligand's minor influence, relative to that of the Cp ligand sphere, on the electronics of the lanthanide center. Significant deviations occur at samarium and Eu (and less so at Tm and Yb), where the Ln-centered spin densities increase (or decrease) as a filled or half-filled 4f manifold becomes accessible. This is expected given the relative stability of these elements in their divalent oxidation states.

Table 2 lists the NPA-derived effective electronic configurations of the Ln ions in base-free Cp_3Ln. The 6s and 5d-orbital populations represent electron density formally donated to the Ln^{3+} ion by the three Cp^- anions. The 4f-orbital populations primarily correspond to the expected number of Ln-centered, non-bonding electrons, although these numbers are elevated by almost 0.2 electrons for the early lanthanides which is apparently because of a small f-orbital/Cp interaction (the Cp_3 ligand set has the appropriate C_3 symmetry and the f-orbitals are less contracted early in the Ln period). A feature that is obscured in the total spin density values shown above is manifest at terbium and dysprosium, where roughly 0.5 e^- is promoted from the 4f manifold to the 6s orbital: in these species one of the non-bonding Ln-centered orbitals is predicted to be essentially an sf hybrid. What is important to note from these data is that the d-orbital populations are relatively invariant and close to 1. This suggests that while the Cp_3Ln species contain a formally trivalent metal ion, from the "viewpoint" of a dative ligand the lanthanide center might be better described as divalent, with an $f^{(n-3)}d^1$ electronic configuration (where n = 3 for La, etc.) which is an excited state for free Ln^{2+} (except La^{2+} and Gd^{2+}).

Tables 3 and 4 list Ln electronic configurations and lanthanide-centered acceptor-orbital hybridizations derived from NLMO analyses on all $Cp_3Ln-AlCp$ and $Cp_3Ln-GaCp$ adducts, respectively. Not surprisingly, the 6s and 5d-orbital populations are only moderately higher than those in the non-ligated Cp_3Ln complexes,

Table 2. Calculated Ln NPA Electron Configurations in Cp_3Ln

Ln[a]	e^- config.[b]	Ln[a]	e^- config.[b]
La	$6s^{0.10}\ 5d^{1.14}\ 4f^{0.17}$	Tb	$6s^{0.74}\ 5d^{1.33}\ 4f^{7.43}$
Ce	$6s^{0.11}\ 5d^{1.19}\ 4f^{1.20}$	Dy	$6s^{0.67}\ 5d^{1.25}\ 4f^{8.53}$
Pr	$6s^{0.11}\ 5d^{1.19}\ 4f^{2.21}$	Ho	$6s^{0.14}\ 5d^{1.25}\ 4f^{10.08}$
Nd	$6s^{0.06}\ 5d^{0.63}\ 4f^{3.11}$	Er	$6s^{0.14}\ 5d^{1.22}\ 4f^{11.08}$
Pm	$6s^{0.12}\ 5d^{1.21}\ 4f^{4.20}$	Tm	$6s^{0.23}\ 5d^{1.69}\ 4f^{12.13}$
Sm	$6s^{0.12}\ 5d^{1.16}\ 4f^{5.31}$	Yb	$6s^{0.14}\ 5d^{1.05}\ 4f^{13.32}$
Eu	$6s^{0.11}\ 5d^{1.01}\ 4f^{6.52}$	Lu	$6s^{0.15}\ 5d^{1.06}\ 4f^{14.00}$
Gd	$6s^{0.41}\ 5d^{1.15}\ 4f^{7.02}$		

[a] Ln in Cp_3Ln. [b] 0.01 electron cutoff.

indicating that the majority of excess electron density relative to the free Ln^{3+} ions is a consequence of donation from the Ln-bound Cp^- anions (see above). However, the increase in d-orbital population upon CpE binding is significant (about 0.4 e^-) which reflects the strong donor ability of the CpE ligand. As in the Cp_3Ln complexes, the s-orbital populations at Tb and Dy are raised because of s/f hybridization in one of the Ln-centered non-bonding levels.

In the NBO framework, the formally empty lanthanide-centered orbital that accepts electron density from the CpE donor lone pair is a hybrid that can have mixed s, d, and f character. Importantly, the acceptor hybrids calculated here and listed in the third column of Tables 3 and 4 show a predominant d character; a slight contribution from the f-orbital manifold vanishes upon approaching the end of each half-period. These data are consistent with the results of a related study concerning $Cp_3U(IV)-X$.[48] We note that, as in the Tb and Dy adducts, in the Gd species the 6s orbital plays an important role; however, because of Gd's stable $4f^7$ electronic configuration it is in this case the dative bond-acceptor orbital that displays increased s-hybridization instead of the f-orbital manifold.

Considering that the data presented in Table 2 for Cp_3Ln indicates an effectively divalent Ln^{2+} ion with an $f^{(n-3)}d^1$ electronic configuration, we posit that coordination of CpE represents the partial reduction of a Ln^{2+} center to an $f^{(n-3)}d^2$ electronic configuration. While the invocation of a monovalent Ln^+ ion in $Cp_3Ln-ECp$ appears far-fetched, the proposed ligand-to-metal charge donation is small based on experimental observations and so this formalism can be considered a minor (yet useful) resonance form for the adducts. Certainly this formalism explains the weak bonding observed here for a very electron-donating ligand: reduction of a divalent Ln^{2+} ion is quite unfavorable. Likewise, strong sharing of electron density between two electropositive metals need not result in a particularly stabilizing interaction.

6. Bond Indices and CpE→Ln Charge Transfer. With the orbital character of the L→Ln donor−acceptor interaction estimated, we seek to quantify the charge transfer, or covalent, component of the Ln−E bond. Various bond order (*BO*) indices have been proposed but in lanthanide bonding the meaning of any given reported number, or its bearing on the strength of the Ln-ligand interaction, is unclear.[49] This is especially true in metal−metal multiple

(48) Ben Yahia, M.; Belkhiri, L.; Boucekkine, A. *J. Mol. Struct.* (*THEOCHEM*) **2006**, *777*, 61–73.

(49) (a) Jonas, V.; Frenking, G.; Reetz, M. T. *J. Am. Chem. Soc.* **1994**, *116*, 8741–8753. (b) Jules, J. L.; Lombardi, J. R. *J. Mol. Struct.* (*THEOCHEM*) **2003**, *664*, 255–271. (c) Tobisch, S.; Nowak, T.; Bogel, H. *J. Organomet. Chem.* **2001**, *619*, 24–30.

Table 3. Lanthanide NPA Electron Configurations and NLMO CpAl→Ln Acceptor-Orbital Hybridizations in $Cp_3Ln-AlCp$

[Ln]-AlCp[a.]	Ln e^- config.[b.]	E→Ln σ-acceptor hybrid (%)[c.]	[Ln]-AlCp[a.]	Ln e^- config.[b.]	E→Ln σ-acceptor hybrid (%)[c.]
La	$6s^{0.19}\ 5d^{1.51}\ 4f^{0.17}$	22.6s, 72.5d, 4.8f	Tb	$6s^{0.82}\ 5d^{1.77}\ 4f^{7.44}$	20.1s, 75.9d, 3.6f
Ce	$6s^{0.20}\ 5d^{1.57}\ 4f^{1.19}$	22.9s, 72.3d, 4.6f	Dy	$6s^{0.75}\ 5d^{1.75}\ 4f^{8.53}$	21.0s, 74.9d, 3.6f
Pr	$6s^{0.20}\ 5d^{1.60}\ 4f^{2.19}$	22.6s, 73.6d, 3.6f	Ho	$6s^{0.23}\ 5d^{1.75}\ 4f^{10.07}$	21.9s, 76.7d, 0.9f
Nd	$6s^{0.20}\ 5d^{1.59}\ 4f^{3.18}$	23.3s, 73.4d, 3.0f	Er	$6s^{0.23}\ 5d^{1.74}\ 4f^{11.06}$	22.2s, 76.8d, 0.6f
Pm	$6s^{0.21}\ 5d^{1.60}\ 4f^{4.17}$	23.2s, 74.1d, 2.4f	Tm	$6s^{0.23}\ 5d^{1.69}\ 4f^{12.13}$	22.2s, 76.0d, 1.3f
Sm	$6s^{0.20}\ 5d^{1.54}\ 4f^{5.27}$	23.5s, 72.9d, 3.3f	Yb	$6s^{0.22}\ 5d^{1.56}\ 4f^{13.23}$	22.9s, 75.6d, 1.2f
Eu	$6s^{0.19}\ 5d^{1.33}\ 4f^{6.49}$	27.3s, 72.1d, 0.4f	Lu	$6s^{0.24}\ 5d^{1.63}\ 4f^{14.00}$	23.9s, 75.8d, 0.0f
Gd	$6s^{0.53}\ 5d^{1.62}\ 4f^{7.01}$	43.3s, 56.0d, 0.4f			

[a.] [Ln] = Cp_3Ln. [b.] 0.01 electron cutoff. [c.] 0.2% cutoff, average of α and β spin orbitals.

Table 4. Lanthanide NPA Electron Configurations and NLMO CpGa→Ln Acceptor-Orbital Hybridizations in $Cp_3Ln-GaCp$

[Ln]-GaCp[a.]	Ln e^- config.[b.]	E→Ln σ-acceptor hybrid (%)[c.]	[Ln]-GaCp[a.]	Ln e^- config.[b.]	E→Ln σ-acceptor hybrid (%)[c.]
La	$6s^{0.17}\ 5d^{1.46}\ 4f^{0.18}$	21.8s, 72.9d, 5.2f	Tb	$6s^{0.80}\ 5d^{1.71}\ 4f^{7.44}$	19.7s, 76.6d, 3.3f
Ce	$6s^{0.18}\ 5d^{1.52}\ 4f^{1.20}$	22.5s, 72.6d, 4.8f	Dy	$6s^{0.73}\ 5d^{1.68}\ 4f^{8.53}$	19.9s, 76.8d, 3.0f
Pr	$6s^{0.18}\ 5d^{1.54}\ 4f^{2.19}$	22.3s, 73.9d, 3.6f	Ho	$6s^{0.20}\ 5d^{1.67}\ 4f^{10.07}$	20.9s, 77.9d, 0.8f
Nd	$6s^{0.18}\ 5d^{1.56}\ 4f^{3.17}$	22.0s, 74.9d, 2.9f	Er	$6s^{0.20}\ 5d^{1.66}\ 4f^{11.07}$	20.7s, 78.4d, 0.5f
Pm	$6s^{0.19}\ 5d^{1.55}\ 4f^{4.18}$	23.1s, 74.5d, 2.2f	Tm	$6s^{0.20}\ 5d^{1.60}\ 4f^{12.14}$	20.8s, 77.8d, 1.1f
Sm	$6s^{0.18}\ 5d^{1.48}\ 4f^{5.28}$	23.4s, 73.6d, 2.8f	Yb	$6s^{0.19}\ 5d^{1.46}\ 4f^{13.27}$	21.7s, 77.8d, 0.2f
Eu	$6s^{0.17}\ 5d^{1.29}\ 4f^{6.50}$	26.1s, 73.2d, 0.4f	Lu	$6s^{0.21}\ 5d^{1.55}\ 4f^{14.00}$	21.7s, 78.1d, 0.0f
Gd	$6s^{0.47}\ 5d^{1.50}\ 4f^{7.02}$	33.9s, 65.4d, 0.4f			

[a.] [Ln] = Cp_3Ln. [b.] 0.01 electron cutoff. [c.] 0.2% cutoff, average of α and β spin orbitals.

bonding,[50] for instance CASPT2 calculations (including spin orbit effects) on the actinide dimers indicate that Pa_2 and U_2 have similar effective *BO*s (4.5 and 4.2, respectively) but the bond energy of the former is almost four times larger than that of the latter.[51] More relevantly, in the analysis of a U(IV)−Ga(I) interaction it was suggested that π-electron donation from the Ga center contributed to the U−Ga *BO* although it is unlikely that such an interaction stabilizes the bond significantly.[52] That being stated, because all Ln-ligand interactions studied here are of the same type (one-donor orbital, one-acceptor orbital σ-bonds), trends in *BO* indices may be amenable to comparison with trends in bond strengths across the lanthanide series (see section 7).

Figure 7a charts the NLMO/NPA bond orders[53] computed for the $Cp_3Ln-ECp$ adducts. This particular *BO* index was chosen mainly for consistency not only because it is derived from the NBO formalism used here but also because in this case it yields the smallest and thus probably the most realistic values. The calculated *BO*s correlate inversely with the Ln−E bond lengths (see Figure 2). Generally, lanthanides of the second half of the period are predicted to exhibit stronger Ln−E covalent bonding than those of the first half (Eu being the most weakly bonding), with Lu being the most strongly interacting of the series if the $Cp_3Gd-AlCp$ datum is disregarded. The Gd−Al point is an outlier, and illustrates how a deviation in bond length can result in a large deviation in calculated *BO* while other properties investigated here are much less affected.

In a related study of an anionic R_3Si^- ligand, Zeckert and co-workers calculated NRT-derived bond orders of 0.38 and 0.46 for the Cp_3La and Cp_3Yb adducts, respectively,

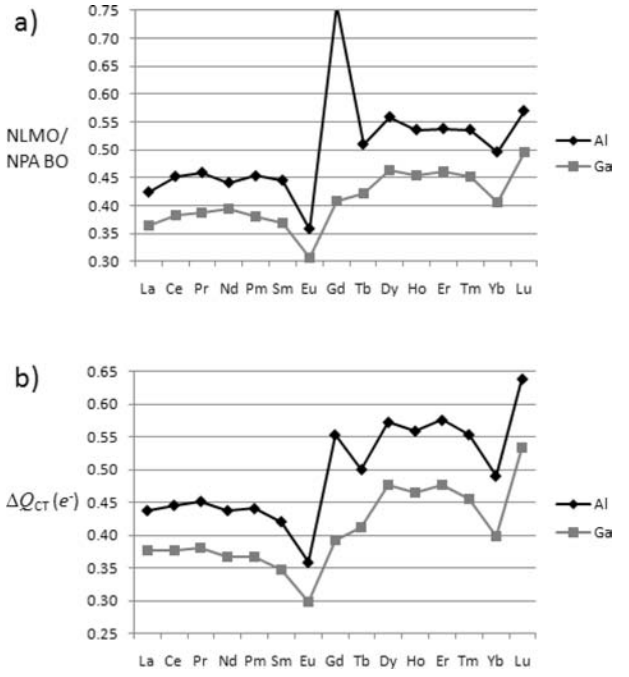

Figure 7. (a) NLMO/NPA Ln−E bond orders in $Cp_3Ln-ECp$. (b) CpE→Ln charge transfer, defined as $\Delta Q_{CT} = Q_{(Free)} - Q_{(Bound)}$, Q = natural charge on Ln, *Free* = Cp_3Ln, and *Bound* = $Cp_3Ln-ECp$.

using the BP86 functional and a basis set of similar quality to that used here.[54] Those data are consistent with the *BO* trend observed in the current system; however, their calculated Wiberg bond indices showed opposite behavior (0.37 and 0.30, respectively). For comparison we report Wiberg values of 0.54/0.59 for $Cp_3[La/Yb]-AlCp$ and 0.46/0.47 for $Cp_3[La/Yb]-GaCp$, which agree with the NLMO/NPA and NRT *BO* trends (although the case of CpGa is ambiguous).

(50) Wagner, F. R.; Noor, A.; Kempe, R. *Nat. Chem.* **2009**, *1*, 529–536.
(51) Roos, B. O.; Malmqvist, P. A.; Gagliardi, L. *J. Am. Chem. Soc.* **2006**, *128*, 17000–17006.
(52) Liddle, S. T.; McMaster, J.; Mills, D. P.; Blake, A. J.; Jones, C.; Woodul, W. D. *Angew. Chem., Int. Ed.* **2009**, *48*, 1077–1080.
(53) Reed, A. E.; Schleyer, P. v. R. *J. Am. Chem. Soc.* **1990**, *112*, 1434–1445.
(54) Zeckert, K.; Zahn, S.; Kirchner, B. *Chem. Commun.* **2010**, *46*, 2638–2640.

Because ligand-to-metal dative bonding between elements of similar *EN* is primarily a charge-transfer (*CT*) phenomenon, the difference in Ln-centered charge between its CpE-ligated and unsaturated state should provide information similar to the bond orders discussed above. The extent of the *CT* interaction can be approximated by subtracting the Ln ion's natural charge in the CpE adduct from that in the corresponding free Cp_3Ln complex. Accordingly, E→Ln *CT* parameters ΔQ_{CT} were calculated (shown in Figure 7b, see caption for the definition) and were found to closely reproduce the behavior of the *BO*s. The correlations between *BO*s and ΔQ_{CT} values are nearly quantitative, with linear fits having R^2 values of 0.94 and 0.96 for the CpAl and CpGa series, respectively (see Supporting Information, Figure S12, Gd data removed).

Both NLMO/NPA *BO* and ΔQ_{CT} metrics predict trends that are quite similar to that found for the molecular dipole moments, reported in section 4, if one adds a correction to the dipole values which increases monotonically across the lanthanide series (see below). This in turn suggests that the trend in molecular dipole moment arises from changes in relative E→Ln charge transfer strength rather than changes in lanthanide *EN* (which should be monotonic).

7. Ln-E Bond Disruption Thermodynamics. From the data presented above it is clear that Ln-ligand bonding in $Cp_3Ln-ECp$ is controlled by factors more subtle than simple electrostatic interactions with trivalent metal ions of smoothly decreasing radius and monotonically increasing electronegativity. These factors are foreshadowed in the correlations observed between various quantities including *d*(Ln−E), molecular dipole moment, and $BO/\Delta Q_{CT}$ presented in previous sections. That all of these trends are correlated (some inversely) strongly suggests that they are all consequences of the same fundamental property. It follows that if the metrics discussed above are indicators of relative metal−ligand interaction strength then the Ln−E *BDE*s should also be determined by that same property, as with the metal-to-ligand donor strengths in the bis(arene) adducts. We have proposed that this property is related to the Ln 4f and 5d-orbital energy levels, and an indication of the relevant orbital interactions was given in section 5.

To our knowledge orbital promotion energies have not been employed to rationalize ligand-to-metal donor interactions in formally trivalent lanthanide compounds. Where filled d states in the zero-valent lanthanides act as electron donors, those states are unoccupied in the trivalent ions and thus can act as acceptors. Therefore, as the Ln^0 f→d promotion energies can be used to predict the metal-to-ligand dative bond strength in the bis(arene) species, it might be logical to suggest that those same transitions of the Ln^{3+} ions could be used to predict the Ln−E *BDE*s in $Cp_3Ln-ECp$ (where the *BDE* is *inversely* proportional to the promotion energy). However, the literature values[47] for the f→d promotion energies of Ln^{3+}, reproduced in Figure 8, clearly do not agree with the behavior predicted in the previous sections. Specifically, Gd and Lu would be predicted to have the lowest Ln−E *BDE*s of the series.

Using the promotion energies for the divalent ions mitigates this problem (at least for Gd) but still only

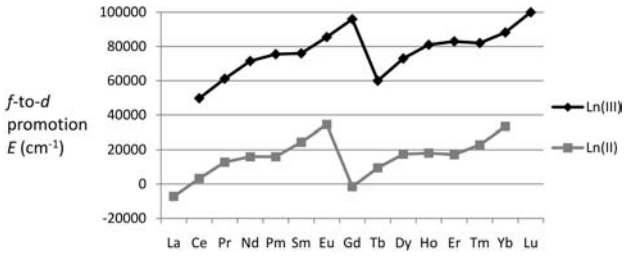

Figure 8. Literature values for the f→d promotion energies of the Ln^{3+} and Ln^{2+} ions. Negative values indicate ground states with occupied d levels.

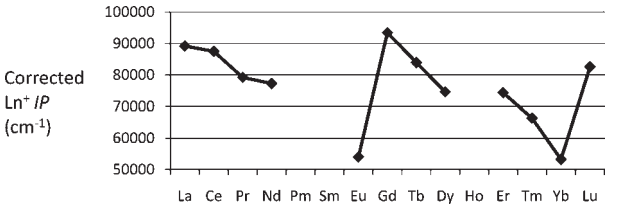

Figure 9. Second ionization potentials of Ln atoms corrected for excitation energies from the Ln^+ ground state to the $f^{(n-3)}d^2$ state.

provides the 5d-orbital energies *relative* to the 4f manifold. Further examination of the bonding model proposed in section 5 is warranted. If the relevant process during heterolytic Ln−E bond cleavage is removal of electron density from a 5d orbital on a formally $f^{(n-3)}d^2$ Ln^+ center then the energy required to do so would correlate with the ionization potential (*IP*) of the Ln^+ ion in that electronic state. Accordingly, Figure 9 illustrates the result of subtracting, from the ionization potential of each Ln^+ ion, the excitation energy from its ground state to its $f^{(n-3)}d^2$ state, where such excitation energy values are available.[47a] Note that Eu and Yb comprise the minima of the series (equivalent to maxima in Figure 8), and the early lanthanides exhibit much attenuated values (relative to the later elements) compared with the promotion energies referenced above. The data presented in Figure 9 aids in explaining the increased participation of Gd's 6s orbital in its dative-ligand acceptor hybrid: at this point in the series the d-s orbital energy separation should be at a minimum. Additionally, this trend can be directly compared with those used to predict bond strengths in this case because a larger *IP* corresponds to a more tightly bound electron (or donor ligand);[55] indeed, this plot is strikingly similar to the plots of predicted molecular dipole moment (see Figure 4) which we proposed are predictive of the Ln−E *BDE*s. Obviously, a direct computational measure of the trend in Ln−E *BDE* would be very desirable as a means of supporting this claim.

The measured Ce−Ga *BDE* of $(CpSiMe_3)_3Ce-GaCp^*$ reported in section 2 afforded the opportunity to test the predictive utility of the computational methods described in our previous report. In that study, it was discovered that averaging the differences between the *BDE* values for the $Cp_3[U/Nd]-GaCp$ model adducts and those found experimentally for the real complexes $(CpSiMe_3)_3[U/Nd]-GaCp^*$ yielded a correction factor of 0.9 kcal mol^{-1}

(55) A similar argument can be used to rationalize the bond strengths in LnO, which follow the same trend, see: Dolg, M.; Stoll, H. In *Handbook of Chemistry and Physics of Rare Earths*; Gschneidner, K. A., Eyring, L., Eds.; Elsevier: Amsterdam, 1996; Vol. *22*, pp 607−729.

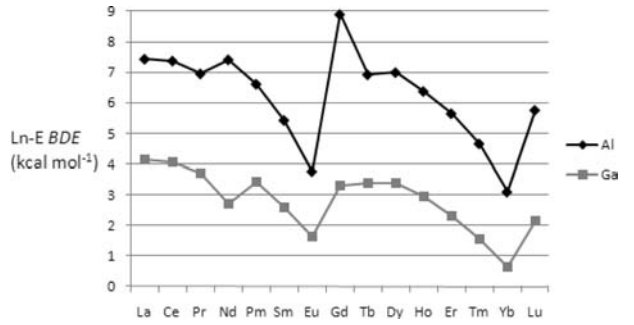

Figure 10. Predicted Ln−E *BDE*s for $(CpSiMe_3)_3Ln-ECp^*$ (E = Al, Ga; from corrected model $Cp_3Ln-ECp$ values; in kcal mol^{-1}). Larger values correspond with more strongly bound adducts.

when using the B3PW91 functional. *Adding* that correction to the calculated *BDE* values for the analogous CpAl model adducts allowed the accurate prediction of the *BDE*s for $(CpSiMe_3)_3$[U/Nd]−AlCp*. Note that such a small correction should not be taken as evidence that B3PW91 intrinsically treats this system accurately, as the values were obtained using simplified models which may display quite different *BDE*s than the fully substituted adducts. This model chemistry, when applied to $Cp_3Ce-GaCp$, yielded a predicted *BDE* of 4.1 kcal mol^{-1} for $(CpSiMe_3)_3Ce-GaCp^*$ which is in excellent agreement with the experimental value of 4.2(1) kcal mol^{-1} (here we define *BDE* as positive for a stabilizing interaction). With such a favorable result in hand, these methods were extended to the other isostructural adducts in the lanthanide series, under the assumption that this additive factor is constant for all isostructural lanthanide adducts.

Figure 10 displays the predicted Ln−E *BDE*s (ΔH_{0K}) for all compounds $(CpSiMe_3)_3Ln-ECp^*$. Gratifyingly, the overall trend in the *BDE* values matches reasonably closely that for the (corrected) second *IP* data shown in Figure 9, with values decreasing across the first half of the period, increasing markedly at Gd, and again decreasing through Yb before spiking at Lu. Likewise, the progression across the series also correlates well with that for the molecular dipole moments. Special attention must be paid to the values at Nd and Gd, where the Al data break the trend to higher values relative to those of their neighbors whereas the Ga data similarly break the trend to lower values. Since the Ce−Ga and Nd−Ga data correspond with the experimental values they are obviously not in error. This suggests that it is actually the [Pm−Eu]−Ga and [Nd−Eu]−Al data that are overestimated, which is reasonable given that these species are likely to suffer from the use of a single-determinant model chemistry (see section 3). In the Gd case, the *IP* value (relative to the others in the series) is intermediate between those predicted here for the Cp*Al and Cp*Ga adducts. This evidence is circumstantial but does suggest that the Gd adducts may actually be the most stable in each series although the Al and Ga values are over- and underestimated, respectively. Therefore the most weakly binding adducts are predicted to be those with Yb, and the most strongly binding are those with lanthanides at the beginning of each half-period. This ordering opposes that found computationally for two divalent $Cp^*_2Ln-AlCp^*$ complexes, where the Yb adduct was predicted to be slightly more stable than its Eu analogue.[17c] It is not clear

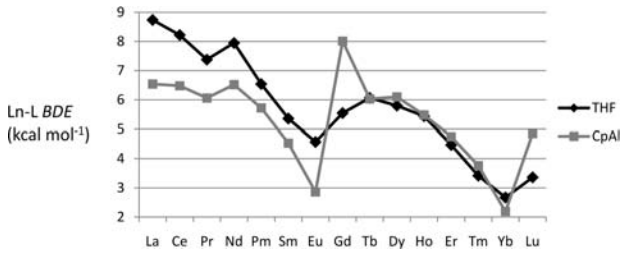

Figure 11. Comparison of uncorrected Ln−L *BDE*s (ΔH_{0K}) for $Cp_3Ln-THF$ and $Cp_3Ln-AlCp$, in kcal mol^{-1}.

whether the discrepancy is due to "noise" in the computed values or if the presence of formally Ln^{2+} ions in the other study significantly changes the intrinsic ordering; we do note that the difference in (corrected) second *IP* values for Eu and Yb is very small, and the estimated errors in the tabulated data are quite large.

All of the calculated data presented here ultimately derive from the electron density, and it has not yet been proven that the trends discussed above do not all arise from artifacts caused by the use of ECPs, and so forth. Accordingly, Ln−THF *BDE*s were also calculated for the $Cp_3Ln-THF$ adducts discussed in section 3 and compared with the (uncorrected) values for $Cp_3Ln-AlCp$ in Figure 11. The values are probably quite underestimated relative to the true *BDE*s given the extreme overestimation of the Ln−O bond lengths (see above). However, here this is actually advantageous because a more weakly binding system is more likely to exhibit spurious behavior. While the Ln−THF *BDE*s clearly deviate from a linear trend across the period (in a manner similar to the Ln−E *BDE*s), those for the adducts early in the first and second half-periods (and that for Lu) do approximately define a linear trend; that is, the early lanthanides are unambiguously predicted to form stronger adducts with THF than those in the second half-period. Moreover, in this case the deviations in Ln−L *BDE* inversely correlate with the deviations in *d*(Ln−O) which contrasts sharply with the data for CpE adducts. This observation lends support to the argument that the relative bond strength is directly related to the bond length in adducts containing hard Lewis bases but not soft bases. Again, it must be stressed that under-binding of the THF adducts in this model chemistry probably exaggerates the relative covalent character of the THF→Ln dative bond, assuming that electrostatic interactions are dominant in determining the bond strengths in those adducts. We take the absence of strongly bimodal character in the trans-period Ln−L bonding trend for the hard-donor ligand THF as strong evidence that the behavior of the $Cp_3Ln-ECp$ series is indeed physical, and only observed because in this case the covalent bonding component is not masked by a dominant electrostatic component.

To reiterate, the trends in *BDE* and molecular dipole moment are quite similar and appear to be predictable from the (Ln^+ excitation energy-corrected) second ionization potentials of the Ln atoms. However, as the Ln series is progressed their correlation with those for *BO* indices and *CT* metrics degrades: the values relative to those at the beginning of the period are increasingly attenuated. A possible cause of this attenuation is illustrated by decomposition of the *BDE* values into the magnitude of the

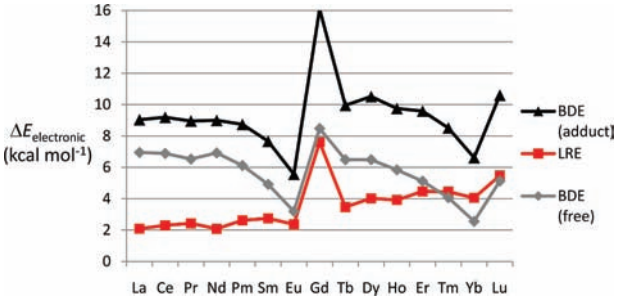

Figure 12. *BDE*(adduct): non-relaxed Ln−E bond disruption energy, relative to fragments in their adduct geometries, higher values signify stronger bonding. *LRE*: ligand reorganization energy upon Ln−E binding, higher values are more unfavorable. *BDE*(free): relaxed Ln−E bond disruption energy, using fragments in their relaxed geometries, higher values signify stronger bonding. No ZPE or empirical corrections were added.

bonding interaction between the metal and the ligand fragments in their adduct geometries and the energy needed to reorganize the fragments from their preferred geometries in the dissociated state. We define the needed terms as follows: *BDE*(adduct) refers here to the bond disruption *energy* (electronic *E* only) when the two fragments are separated while retaining their non-relaxed adduct geometries. *LRE* is the ligand reorganization *energy*, which is the energy expended in distorting the ligand-sphere geometry of both fragments to their adduct geometries. Finally, *BDE*(free) refers here to the net bond disruption *energy* (the enthalpies presented earlier with the ZPE and empirical corrections removed), which is necessarily defined as *BDE*(free) = *BDE*(adduct) − *LRE*, where both *BDE*(adduct) and *LRE* are positive.

Figure 12 depicts the result of separating the metal−ligand binding and ligand reorganization components of the net bond disruption energies of Cp_3Ln−AlCp (recalculation of every Cp_3Ln and ECp fragment at each adduct geometry rendered analysis of both Al and Ga analogues prohibitively expensive). Unlike net bonding energies *BDE*(free), the *BDE*(adduct) values more closely correlate with the *BO*/*CT* data (although the agreement is still mediocre) and *less* closely with the experimental (corrected) *IP* values. This obviously presents a conundrum, as an additional stabilizing effect must then be invoked which balances the *LRE* in order bring the *BDE*s back into agreement with the *IP*s. That is, the observed *BDE* is determined by the (corrected) *IP as well as* an additional factor. Assuming that this factor is not simply an artifact of the computational method, it is likely the very same influence responsible for the destabilizing *LRE* effect: the lanthanide contraction. The contraction is mainly determined by the radial extent of the 5p orbitals, and because the 5d manifold contracts less rapidly across the period than does the 5p manifold (partially because of relativistic effects[56]),[57] electron density donated from a ligand to a Ln 5d orbital experiences less core repulsion later in the lanthanide series. In summary, it appears that in this case two effects due to the lanthanide contraction cancel, which allows the trend in Ln−E *BDE* to be predicted fairly well solely on the basis of the second ionization potentials of the Ln atoms (corrected for the effective electronic states of the Cp_3Ln complexes). In turn, the use of these specific corrected *IP*s presupposes that the dominant Ln−E bonding interaction is a covalent charge transfer.

As an aside, it should be noted that the entropy changes ΔS upon Ln−E bond formation that were presented in section 2 have been disregarded in the theoretical discussion. These values were found to lie in the range of −29 to −31 cal mol^{-1} K^{-1} for the Cp_3Ln−ECp model systems and were approximately invariant across the period (see the Supporting Information, Table S18). Therefore, in the gas phase the ΔS value is predicted to be solely determined by the change in molecularity of the system. The low values of about −9 to −13 cal mol^{-1} K^{-1} derived for $(CpSiMe_3)_3M$−GaCp* are probably then due to solvent effects, where the entropy decrease due to the solvent ordering needed to effectively solvate the free Cp*Ga ligand's electron lone pair partially offsets the entropy increase upon adduct dissociation. That such a strong solvent effect, relative to the gas phase, should be observed in a process involving neutral species and occurring in a nonpolar solvent is remarkable.

Conclusions

Evidence for Cp*Al and Cp*Ga adducts of the trivalent lanthanide complex $(CpSiMe_3)_3Ce$ has been presented, the gallium analogue having been shown to exhibit a slightly higher heterolytic Ln−Ga *BDE* than the isostructural Nd−Ga adduct. That finding prompted a comprehensive computational study of the model compounds Cp_3Ln−ECp (E = Al, Ga) wherein some commonly employed metrics of bonding interactions were evaluated. All data indicate that the trend in Ln−E interaction strength follows a saw-tooth pattern with minima at Eu and Yb, and calculated *BDE*s suggest that the CpE→Gd donor−acceptor interaction may be the strongest in the series. It was found that the second ionization potentials of the Ln atoms (when corrected for the promotion energy to the $f^{(n-3)}d^2$ electronic state in Ln^+) predict the trend in Ln−E *BDE*; however, a correction must be applied to account for the stabilizing effect of a contraction in the Ln core orbital extent across the period. However, in this case that correction is negated by an increasing steric strain on moving across the Ln series.

The predictive use of these ionization potentials necessitates that the primary Ln−E bonding interaction is of the charge-transfer type which in turn indicates that covalency does exist in dative bonding with the formally trivalent Ln^{3+} ions. Nonetheless, this does *not* imply that covalent interactions are an important component of a *strong* bond with a Ln^{3+} ion, as the covalent interactions observed here are exceedingly weak. To state matters differently, significant "electron sharing" need not result in a strong interaction if those shared electrons are not tightly bound to either partner.

The data presented in the previous sections illustrate some pitfalls of commonly used phenomenological probes of bonding interactions. For example, in this case differences in molecular dipole moment probably arise from the relative ligand-to-metal charge transfer strengths and so they are not really a measure of electrostatic contributions to bonding. While bond order indices and changes in metal-centered charge do appear to be qualitatively predictive of metal−ligand bond

(56) Pyykkö, P. *Chem. Rev.* **1988**, *88*, 563–594.
(57) (a) Siekierski, S. C.; Burgess, J. *Concise Chemistry of the Elements*; Horwood: Coll House, Westergate, Chichester, West Sussex, U.K., 2002. (b) Lloyd, D. R. *J. Chem. Educ.* **1986**, *63*, 502–503.

strength, or at least of general trends therein, they do not take into account potentially important ligand strain effects and also appear to be overly sensitive to bond length differences. Moreover, the absolute magnitudes of bond order indices in this type of system should not be considered at all realistic. The current study demonstrates the importance of a synergistic relationship between experiment and theory in f-element chemistry, wherein measured results were used to develop a computational methodology that was subsequently employed to make predictions amenable to experimental verification. Finally, results presented here lend support to the view that the trivalent lanthanides are more than just size-tunable trications with interesting spin properties:[58] changes in the p and f-orbital manifolds indirectly influence molecular properties by perturbing the orbitals that can take part in covalent interactions.

Acknowledgment. We thank R. A. Andersen and O. Eisenstein for important discussions. All computations were performed at the UC Berkeley Molecular Graphics and Computation Facility, directed by Kathleen Durkin, using equipment purchased with funds from NSF Grant CHE-0840505 and donations from Dell.

Supporting Information Available: Crystallographic data for $(CpSiMe_3)_3Ce$ (CIF), additional experimental details, raw data for the experimental determination of M−E binding constants, tables of all computed data presented as plots, coordinates and energies for all computed structures, complete Gaussian citation. This material is available free of charge via the Internet at http://pubs.acs.org.

(58) Evans, W. J. *Inorg. Chem.* **2007**, *46*, 3435–3449.